Available online at www.sciencedirect.com
SCIENCE DIRECT®
Int. J. Miner. Process. 72 (2003) 227–237
INTERNATIONAL JOURNAL OF MINERAL PROCESSING
www.elsevier.com/locate/ijminpro

Calculation of the flotation rate constant of chalcopyrite particles in an ore

J. Duan, D. Fornasiero, J. Ralston*

Ian Wark Research Institute, The ARC Special Research Centre for Particle and Material Interfaces, University of South Australia, Mawson Lakes, Adelaide S.A. 5095, Australia

Received 24 January 2003; received in revised form 19 June 2003; accepted 30 June 2003

Abstract

The flotation recovery of chalcopyrite particles in a complex sulfide ore was measured in a Rushton turbine flotation cell as a function of particle size. The experimental flotation rate constants of these particles were compared to those calculated using a recently developed flotation model that incorporates contributions from the efficiencies of collision, attachment and stability between particles and bubbles, as well as their frequency of collision. For these calculations, the contact angle of the chalcopyrite particles in the ore was obtained independently using an approach based upon Time of Flight Secondary Ion Mass spectroscopy (ToF-SIMS). It was found that the calculated flotation rate constants were in good agreement with the experimental data and able to reproduce the characteristic maximum in flotation rate constant for particles of intermediate size. The values of bubble velocity and turbulent dissipation energy derived from these calculations are relatively low and may well correspond to mean values of these parameters inside the flotation cell.

Keywords: flotation; chalcopyrite; turbulence; surface analysis; rate constant

1. Introduction

The prediction of flotation rate constants from first principles is of great importance in mineral processing. The basic processes that govern the rate of recovery, or collection efficiency (E_{coll}), of particles in a flotation cell are well understood and include the consecutive sub-processes of particle–bubble collision, attachment and stability, represented by efficiencies E_c, E_a, E_s, respectively (Derjaguin and Dukhin, 1961),

$$E_{coll} = E_c \cdot E_a \cdot E_s \quad (1)$$

The rate of particle recovery in the froth (or froth efficiency) can also be incorporated in Eq. (1), however, in the present study, it is assumed that it is unity as the froth is very shallow with depth of only a few centimeters (Mular and Musara, 1991). Collision is dominated by bulk hydrodynamics inside the flotation cell (e.g., bubble velocity and turbulence), while attachment is dominated by the interfacial behaviour between the particle and bubble (e.g., particle hydrophobicity influences thin film drainage). As for stability, its efficiency depends on both hydrodynamics and interfacial events. Several models can be used for the calculation of collision, attachment and stability efficiencies; however, their applicability is restricted to the approximations (e.g., fluid flow conditions,

* Corresponding author. Fax: +61-8-83023683.
E-mail address: john.ralston@unisa.edu.au (J. Ralston).

0301-7516/$ - see front matter © 2003 Elsevier B.V. All rights reserved.
doi:10.1016/S0301-7516(03)00101-7

mobility of the bubble surface) inherent to each model (e.g., Dai et al., 2000). The validity of Eq. (1) has been demonstrated in studies involving mostly single mineral flotation experiments in simple flotation columns. With these models, the collection efficiency, or flotation rate constant, of well-defined particles has been calculated as a function of particle size and contact angle, as well as bubble size and velocity (e.g., Dai et al., 1998; Crawford and Ralston, 1988). With mixed minerals or ores, no easy and reliable technique exists for the measurement of the contact angle of a particular mineral in an ore. Recent studies have shown that it is now possible to obtain this information using Time of Flight Secondary Ion Mass spectroscopy (ToF-SIMS) correlated with independent measurements of contact angle (Piantadosi et al., 2000; Pyke et al., 2001; Piantadosi and Smart, 2002).

The objective of this present work is to demonstrate how the flotation rate constants of particles as a function of particle size and contact angle, bubble size and velocity, and level of turbulence inside flotation cell may be calculated. These calculations are then compared with the flotation rate constants of chalcopyrite particles in an ore measured in a Rushton flotation cell of well-known hydrodynamic characteristics. The contact angle of the chalcopyrite particles in the ore will be determined by ToF-SIMS, using an appropriate calibration procedure.

2. Theoretical background

2.1. Flotation rate constant

The rate of removal of particles by bubbles in a flotation cell is given by (Jameson et al., 1977; Ralston, 1992; Pyke et al., 2003)

$$\frac{dN_p}{dt} = kN_p = -Z_{pb}E_{coll} \tag{2}$$

where k is the flotation rate constant and E_{coll} is given by Eq. (1).

Z_{pb} is the collision frequency per unit volume between particles and bubbles of diameters d_p and d_b, respectively (e.g., Abrahamson, 1975; Schubert, 1999),

$$Z_{pb} = 5N_pN_bd_{pb}^2\sqrt{\overline{V}_p^2 + \overline{V}_b^2} \tag{3}$$

where N_p and N_b are the number densities of floatable particles and bubbles, respectively. $d_{pb}=(d_p+d_b/2)$ and $(\overline{V}_p^2)^{1/2}$ and $(\overline{V}_b^2)^{1/2}$ are the root mean square (rms) velocity fluctuations of the particles and bubbles relative to the turbulent fluid velocity, respectively.

We note that the term $5d_{pb}^2\sqrt{\overline{V}_p^2 + \overline{V}_b^2}$ in Eq. (3) is the collision volume of fluid that is swept by the bubble per unit time (Jordan and Spears, 1990; Pyke et al., 2003).

The rms relative velocities of the particles and bubbles in the turbulent conditions of the flotation cells can be approximated by the following expression (Schubert and Bischofberger, 1978; Schubert, 1999),

$$(\overline{V}_i^2)^{\frac{1}{2}} = \frac{0.33\varepsilon^{\frac{4}{9}}d_i^{\frac{7}{9}}}{\upsilon^{\frac{1}{3}}}\left(\frac{\Delta\rho}{\rho_{fl}}\right)^{\frac{2}{3}} \tag{4}$$

where the subscript i refers to the particle or bubble, ε is the turbulent dissipation energy and $\Delta\rho$ is the difference between the particle and fluid densities.

For $d_b \gg d_p$, then d_p and $\overline{V}_p^2$ can be neglected and $d_{pb} \sim (d_b/2)$.

Thus,

$$Z_{pb} \approx 5N_pN_b\left(\frac{d_b}{2}\right)^2\left[\frac{0.33\varepsilon^{\frac{4}{9}}d_b^{\frac{7}{9}}}{\upsilon^{\frac{1}{3}}}\left(\frac{\Delta\rho}{\rho_{fl}}\right)^{\frac{2}{3}}\right] \tag{5}$$

The flotation rate constant k can be obtained by combining Eqs. (2) and (5)

$$k = N_b \cdot 5\left(\frac{d_b}{2}\right)^2\left[\frac{0.33\varepsilon^{\frac{4}{9}}d_b^{\frac{7}{9}}}{\upsilon^{\frac{1}{3}}}\left(\frac{\Delta\rho_b}{\rho_{fl}}\right)^{\frac{2}{3}}\right]E_{coll} \tag{6}$$

N_b can be related to the gas flow rate G_{fr} and the residence time t_r of bubbles in the unit volume

$$N_b = \frac{6G_{fr}}{\pi d_b^3 \cdot V_{cell}}t_r \tag{7}$$

where V_{cell} is the volume of the flotation cell. The residence time t_r can also be expressed as the time that the bubbles of velocity v_b remain in the unit volume

$$t_r = \frac{1 \text{ unit length}}{v_b} \tag{8}$$

By combining Eqs. (1), (6), (7) and (8), we obtain the final expression for the flotation rate constant,

$$k = 2.39\frac{G_{fr}}{d_b \cdot V_{cell}}\left[\frac{0.33\varepsilon^{\frac{4}{9}}d_b^{\frac{7}{9}}}{\upsilon^{\frac{1}{3}}}\left(\frac{\Delta\rho_b}{\rho_{fl}}\right)^{\frac{2}{3}}\cdot\frac{1}{v_b}\right]E_c\cdot E_a\cdot E_s$$

mechanical term | primary turbulence term | elementary processes

(9)

There is a strong similarity to the expression of the flotation rate constant for a batchwise flotation process in the absence of turbulence (Jameson et al., 1977; Ralston, 1992),

$$k = \frac{3}{2}\frac{G_{fr}\cdot h}{d_b\cdot V_{cell}}E_c\cdot E_a \tag{10}$$

In this case, h is the height of the flotation cell and E_s is unity. We also note that the expressions for the superficial gas velocity J_g and the superficial surface area rate of bubbles S_b, now used commonly in flotation cell characterization, can be readily introduced in Eq. (9) (Gorain et al., 1996, 1997).

2.2. Collision efficiency, E_c

The Generalized Sutherland Equation (GSE) may be used to predict the efficiencies of bubble–particle collisions under conditions of potential flow over a mobile bubble surface (high Reynolds numbers for the bubble) (Dukhin et al., 1995; Duineveld, 1995; Sam et al., 1996, Dai et al., 1998),

$$E_c = E_{GSE} = E_{c-su}\cdot\sin^2\theta_t \cdot\exp\left\{\left[3K_3\left(\ln\frac{3}{E_{c\text{-}su}}-1.8\right)-\frac{4\left(\frac{2}{3}+\frac{\cos^3\theta_t}{3}-\cos\theta_t\right)}{\sin^4\theta_t}\right]\cos\theta_t\right\} \tag{11}$$

where $E_{c\text{-}su}$ is the Sutherland collision efficiency (Sutherland, 1948), $(\sim 3d_p)/(d_b)$, accounting only for interception and

$$\cos\theta_t = (1+\beta^2)^{1/2}-\beta$$

$$\sin^2\theta_t = 2\beta[(1+\beta^2)^{1/2}-\beta] \tag{12}$$

θ_t is the maximum possible collision angle of the particle on the surface of the bubble beyond which collision is prevented.

The dimensionless number β is a measure of the relative importance of the interceptional and inertial contributions to the collision process in the GSE and is defined as (Dai et al., 1998)

$$\beta = \frac{4E_{c\text{-}su}}{9K_3} \tag{13}$$

where K_3 is defined as

$$K_3 = \frac{v_b(\rho_p-\rho_{fl})d_p^2}{9\upsilon d_b} \tag{14}$$

and υ is the fluid viscosity.

We note that the expression for E_{GSE} was developed for conditions of potential flow over the bubble surface, i.e., where the Reynolds number for the bubble is high. There may be additional modes of particle transport toward the bubble surface that have not been accounted for in present solutions of the particle trajectory equation under turbulent conditions (Dai et al., 1998), which may require additional theoretical and experimental assessment.

2.3. Attachment efficiency, E_a

The attachment model assumes that particle–bubble collision occurs evenly over the section of the bubble surface between angles $\theta=0$ and $\theta=\theta_t$, where the angle θ is measured from the north pole in the case of a rising bubble, and the angle θ_t is the maximum possible collision angle.

A modified Dobby–Finch attachment model (Dai et al., 1999) is used to calculate the attachment efficiency E_a, defined as the ratio of the projected

area corresponding to an angle θ_a, to the projected area corresponding to θ_t

$$E_a = \frac{\sin^2\theta_a}{\sin^2\theta_t} \tag{15}$$

where θ_a, termed the adhesion angle, is the specific collision angle where, if a particle collides with bubble at this angle, its sliding time (t_{sl}) along the surface towards the equator of the bubble equals the induction time (t_{ind}). The angle θ_a relates both the sliding and induction times to the attachment efficiency.

The expression for particle sliding time under potential flow conditions derived by Sutherland (1948) and later by Dobby and Finch (1987) is used to relate the adhesion angle θ_a to the induction time

$$\theta_a = 2 \text{ arc tan exp}\left[-t_{ind}\frac{2(v_p+v_b)+v_b\left(\frac{d_b}{d_p+d_b}\right)^3}{d_p+d_b}\right] \tag{16}$$

Several experimental and theoretical studies have reported a dependency of induction time on particle size (e.g., Jowett, 1980; Ye and Miller, 1988; Li et al., 1990). In a previous study (Dai et al., 1999), we have shown that the induction time can be related to particle size by the following empirical equation

$$t_{ind} = Ad_p^B \tag{17}$$

In that study, we have shown that parameters A and B were independent of the size of particles (diameter less than 80 μm) and bubbles (diameter between 0.7 and 1.5 mm), and solution ionic strength (up to 0.1 M). It was also found that parameter B is a constant ($=0.6\pm0.1$) but the value of A was inversely proportional to the particle contact angle (Dai et al., 1999). The values of these two parameters will be used in the present study to calculate the induction time.

2.4. Particle–bubble stability efficiency, E_s

The efficiency of bubble–particle stability E_s depends on the attachment force between the bubble and the particle in relation to the external stress forces, or detachment forces, in the environment.

The following equation is used to relate E_s to these attachment forces F_{att} and detachment forces F_{det} (Schulze, 1993),

$$E_s = 1 - \exp\left(1 - \frac{F_{att}}{F_{det}}\right) \tag{18}$$

The capillary (on the three-phase contact) and hydrostatic forces constitute the attachment forces while the forces of gravitation, buoyancy and machine acceleration and capillary pressure (in the gas bubble) constitute the detachment forces. The sum of these forces is zero at equilibrium. With the appropriate expressions for these forces, Eq. (18) becomes (Schulze, 1993)

$$E_s = 1 - \exp\left(1 - \frac{|6\gamma\sin\omega\sin(\omega+\varphi)|}{d_p^2(\Delta\rho g+\rho_p a_c)+1.5d_p(\sin^2\omega)f(d_b)}\right) \tag{19}$$

with

$$f(d_b) = \left(\frac{4\gamma}{d_b} - d_b\rho_{fl}g\right) \tag{20}$$

where γ is the surface tension, a_c is the particle centrifugal acceleration in a turbulent flow field, g is the gravitational constant, φ is the particle contact angle and ω ($=180^\circ-\varphi/2$) refers to the location of a particle at the liquid–vapour interface (Huh and Scriven, 1971; Schulze, 1993).

The particle centrifugal acceleration a_c depends on the level of turbulence (ε) in the flotation cell and, as the particle size is smaller than the bubble size, it can be approximated to

$$a_c = 1.9\frac{\varepsilon^{2/3}}{d_b^{1/3}} \tag{21}$$

for large turbulent eddies (Schulze, 1993) or

$$a_c = 29.6\frac{\varepsilon^{2/3}}{d_b^{1/3}} \tag{22}$$

when the eddies and bubble–particle aggregates have similar sizes (Hui, 2001).

Therefore, Eq. (9) and appropriate expressions for E_c, E_a and E_s can be used for the calculation of the flotation rate constant of particles as a function of particle size, density and contact angle, bubble size and velocity, and level of turbulence inside the flotation cell.

3. Experimental section

3.1. Flotation experiment

The characteristics of the Rushton turbine flotation cell used in this study are given in Table 1 (Pyke et al, 2001). The flotation cell is equipped with a stirring impeller whose speed can be controlled and measured accurately using an optical tachometer. Pressurised air was used to generate gas bubbles through a stainless steel frit with pore size of 13 μm at the bottom of the flotation cell.

For the flotation experiments, a Mount Isa Mines (MIM) copper ore was used. The ore contains 4 wt.% chalcopyrite, 6 wt.% iron sulfide minerals (predominantly as pyrite) and 82 wt.% nonsulfide gangue minerals, quartz and dolomite. The ore (1000 g) was ground in a stainless steel Galigher mill with mild steel rods for 20 min at pH 12.5 to produce a feed of particle size d_{80} of around 84 μm. Conditioning and flotation were conducted in the Rushton flotation cell at pH 11.5. After addition of 20 g/ton of frother (DOWFROTH250), a pre-flotation was conducted for 8 min in the absence of collector to remove the carbonaceous pyrite present in the ore. Then, after addition of 50 g/ton of Aero 3477 dialkyl dithiophosphate (DTP) as collector and 5 g/ton of DOWFROTH250, concentrates were collected after 1, 2, 5 and 10 min of flotation (cumulative). Particles in each concentrate and tail sample were then separated into 13 different subsamples of sizes ranging between 2 and 150 μm using sieves, a Warman cyclosizer and a precyclone. Chemical analysis of these samples was performed by Analabs.

Table 1
Rushton turbine flotation cell

Cell dimensions	Impeller specifications
Volume = 2.25×10^{-3} m^3	Six blade Rushton turbine
Diameter = 0.144 m	Diameter = 0.048 m
Height/diameter = 1:1	Width/height/diameter = 5:4:20
Baffle/diameter = 1:10	

A similar flotation experiment was conducted with clean quartz particles of size range similar to that in the ore to determine the level of particle entrainment. The entrainment contribution was subtracted from the particle recovery in each size fraction to obtain the true flotation recovery of the particles in the ore.

3.2. Experimental flotation rate constant

Assuming that the flotation of particles of diameter i follows a first-order rate (see Appendix) reaction, the recovery of these particles, $R_{t,i}$, at time t to a first approximation is given by the following expression

$$R_{t,i} = R_{\max,i}(1 - \exp(-k_i t)) \tag{23}$$

where k_i is the flotation rate constant of particles of diameter i and $R_{\max,i}$ is their flotation recovery at an infinite time.

A nonlinear least square regression was used to calculate k_i and $R_{\max,i}$ from the best fit of the curve of experimental flotation recoveries versus time for each particle size range using Eq. (23). These flotation rate constants are referred in the text as experimental flotation rate constants.

3.3. Laser Doppler Velocimetry

Measurements of fluid velocity and velocity fluctuations were made with a Laser Doppler Velocimetry (LDV) at different positions inside the Rushton flotation cell at the same gas flow rate and stirring speed as in the flotation experiments but in the absence of ore and gas bubbles (Pyke et al., 2003).

The average fluid velocity V_{fl} was calculated from the LDV measurements of velocity vectors in the X, Y and Z directions, V_x, V_y and V_z, respectively, using the expression (Wu and Patterson, 1989)

$$V_{fl} = \sqrt{V_x^2 + V_y^2 + V_z^2} \tag{24}$$

The turbulent dissipation energy ε can be calculated from the expression (Wu and Patterson, 1989)

$$\varepsilon = Aq^{3/2}L^{-1} \tag{25}$$

where $A=0.85$ (Wu and Patterson, 1989; Jenne and Reuss, 1999), L is a measure of the turbulent length macroscale, generally assumed constant and equal to half the turbine depth (0.005 m in this case), and q is the turbulent kinetic energy calculated from the root mean square of the experimental fluctuations of the turbulent fluid velocities in the three directions, $\overline{U}_x$, $\overline{U}_y$ and $\overline{U}_z$, using the expression

$$q = \frac{1}{2}(\overline{U}_x^2 + \overline{U}_y^2 + \overline{U}_z^2). \quad (26)$$

3.4. Time-of-flight secondary ion mass spectrometry (ToF-SIMS)

ToF-SIMS spectra were obtained using a PHI Model 2100 TRIF II system equipped with a gallium liquid–metal ion gun (LMIG) in pulsed mode. The surface of insulating samples was charged compensated using an electron flood gun. The wet mineral samples prepared under the same conditions as in the flotation experiments were mounted onto a piece of indium foil and introduced into the spectrometer preparation chamber. Prior to analysis, the samples were outgassed under vacuum for around 12 h. The primary beam was produced using a gallium gun with a current of 600 pA. An acceleration voltage of 25 kV was used to produce high spatial resolution with a spot size of 0.2 μm. In static mode, the analysis is confined to the top two monolayers. Imaging of the sample involved mapping for positive and negative ions of interest (e.g., DTP, SO_3^-, etc.). Up to 96 chalcopyrite particles from the concentrate sample collected after 2 min of flotation were analysed by ToF-SIMS to obtain statistical information on the amount of hydrophobic (such as DTP) and hydrophilic species (such as hydroxide, oxide, sulfate and sulfite) on their surface (Piantadosi et al., 2000; Piantadosi and Smart, 2002).

3.5. Bubble size determinations

A University of Cape Town (UCT) bubble size analyser was used to determine the bubble size in the flotation cell. The UCT bubble size analyser captures the bubbles and draws them through a glass capillary (diameter, 0.4 mm). Diodes measure the change in refractive index between the water and gas. Using these readings and the volume of gas collected in a burette, the bubble size distribution can be obtained. Up to 4000 bubbles were typically measured using the analyser over a period of 90 s, permitting a statistically significant number of bubbles to be counted. Measurements were performed in duplicate and the analyser data were then compared with photographs.

Agreement between the two techniques was very satisfactory. The mean bubble diameter was 0.97 mm, with a standard deviation of 0.4.

4. Results and discussion

The experimental flotation recoveries for copper as a function of particle diameter and flotation time (after removing the entrainment contribution) are compared in Fig. 1 with the flotation recoveries calculated using Eq. (23). The satisfactory agreement between the experimental and calculated curves validates the use of a first-order rate reaction to describe the flotation process. The flotation rate constants k_i obtained from this fitting exercise are shown in Fig. 2. The trend in flotation rate constant with particle diameter is similar to that observed previously for copper minerals (Lynch et al., 1981) with maximum values obtained for particle diameters near 40 μm. The lower flotation rate constant values of finer and coarser particles have been attributed to the low collision efficiency and low stability efficiency, respectively, of these particles with gas bubbles.

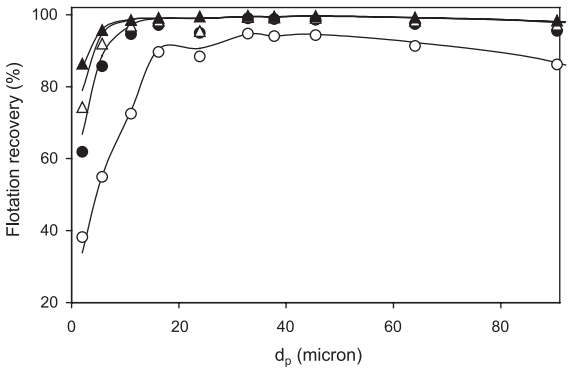

Fig. 1. Experimental (symbols) and calculated (lines) flotation recoveries of chalcopyrite as function of particle diameter and flotation times of 1, 2, 5 and 10 min. A first-order rate equation was used in the calculation of recoveries ([DTP] = 50 g/ton; stirring speed = 720 rpm; $G_{fr} = 5.5 \times 10^{-3}$ m^3/s; $d_b = 0.97$ mm).

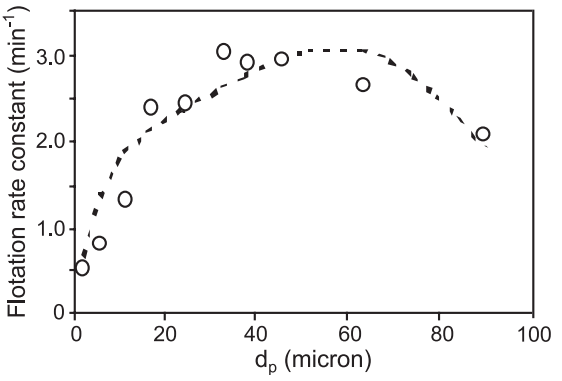

Fig. 2. Experimental (symbols) and calculated (broken line) flotation rate constants of chalcopyrite as function of particle diameter. Eqs. (9)–(22) were used in the calculations of the flotation rate constants ([DTP] = 50 g/ton; stirring speed = 720 rpm; $G_{fr} = 5.5 \times 10^{-3}$ m^3/s; $A = 0.05$; $B = 0.6$; $v_b = 0.2$ m s^{-1}; $\varepsilon = 14$ m^2/s^3; $\rho_p = 4.1$ g cm^{-3}; $d_b = 0.97$ mm).

Eqs. (9)–(22) indicate that only three parameters are required to calculate the flotation rate constant of particles: the turbulent dissipation energy (ε), the bubble velocity (v_b) and the particle contact angle (φ). The value of ε and φ can be independently measured.

4.1. Fluid velocity and energy dissipation in the Rushton flotation cell

Fig. 3 shows the value of the fluid resultant velocity V_{fl} and turbulent dissipation energy ε in the Rushton flotation cell measured by Laser Doppler Velocimetry at a fixed distance of 0.026 m away from the impeller shaft and at different heights above and below the impeller. The results indicate that the value of fluid velocity and energy dissipation is extremely high near the impeller, but small and constant from a height of 0.01 m above the impeller. These measured values are in agreement with values reported in the literature in similar Rushton flotation cells (Wu and Patterson, 1989; Rutherford et al., 1996) and Denver cells (Jordan and Scheiner, 1990).

4.2. ToF-SIMS results

The ToF-SIMS results demonstrated that the DTP collector is selectively adsorbed on the chalcopyrite particles in the MIM ore. However, large differences in the amount and distribution of DTP or oxidation products were observed on the surface of the chalcopyrite particles. This problem was overcome by sampling a large number of these particles to produce a statistical result. Also, the results consistently indicated that the differences in surface chemistry between three size fractions of chalcopyrite (< 10; 20–30 μm; >50 μm) are not statistically significant.

A recent study has shown that ToF-SIMS hydrophobic/hydrophilic indices such as the ratio between the ToF-SIMS signals of DTP and SO_3^- on the surface of a mineral are a good representation of the surface hydrophobicity of that mineral (SO_3^- is the fragment associated with sulfate, representing the hydrophilic species, while DTP represents the hydrophobic collector). Indeed, the flotation recovery, advancing contact angle and ToF-SIMS DTP/SO_3^- index of chalcopyrite particles in single mineral experiments were shown to increase with DTP concentration (Fig. 4) (Pyke et al., 2001).

Using this relationship between advancing contact angle and ToF-SIMS DTP/SO_3^- index established for chalcopyrite particles in single mineral experiments, an advancing contact angle of $71 \pm 2°$ for the chalcopyrite particles in the MIM ore was predicted from a measured ToF-SIMS DTP/SO_3^- index of 9.7×10^{-3} for those particles as shown in Fig. 4.

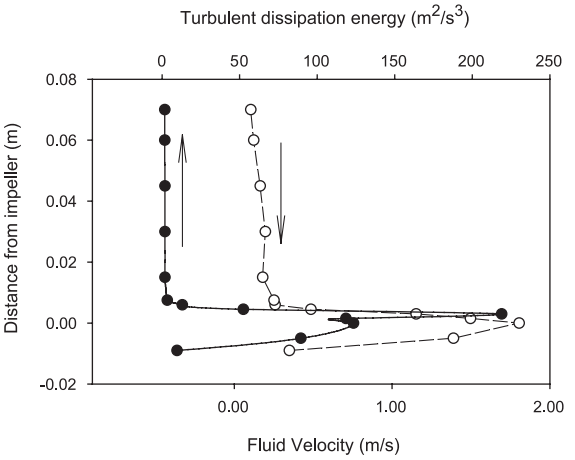

Fig. 3. Fluid velocity V_{fl} (empty circles) and turbulent dissipation energy ε (filled circles) versus vertical distance from the impeller in the Rushton flotation cell and at a fixed distance of 0.026 m away from the impeller axis (stirring speed = 720 rpm).

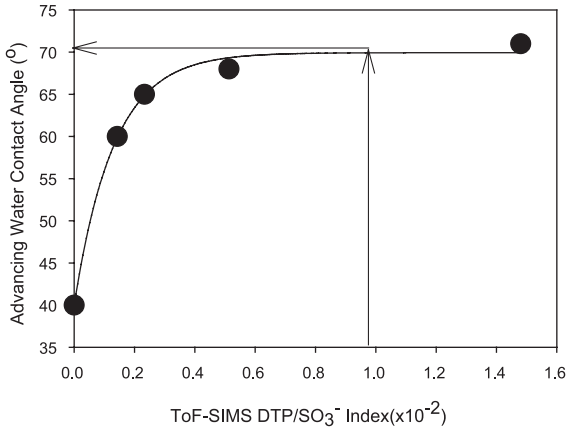

Fig. 4. Relationship between experimental advancing water contact angle and ToF-SIMS DTP/SO_3^- index obtained for chalcopyrite particles in single mineral experiments (Pyke et al., 2001). The arrows indicate the value of contact angle for chalcopyrite particles in the MIM chalcopyrite ore corresponding to a ToF-SIMS DTP/SO_3^- index of 9.7×10^{-3} for these particles. ([DTP] = 50 g/ton).

4.3. Calculation of flotation rate constants

Eqs. (9)–(22) were used to calculate the flotation rate constant as a function of particle diameter. A value of 4.1 g cm^{-3} was used for the density of chalcopyrite (ρ_p). In the calculation of the induction time in Eq. (17), the values of parameter A (dependent on contact angle) and constant B (= 0.6) determined in our earlier study for methylated quartz particles were used (Dai et al., 1999). From an advancing contact angle of 71°, a value of A of 0.05 was extracted from the curve of parameter A versus advancing contact angle (Fig. 5 in Dai et al., 1999).

The calculated flotation rate constant versus particle diameter curves were then compared to the experimental curve in Fig. 2, and a nonlinear least squares program was used to optimise the values of the bubble velocity v_b and turbulent dissipation energy ε until the best fit of the experimental curve was obtained. From these calculations, values of 0.2 m s^{-1} and 14 m^2 s^{-3} were obtained for the bubble velocity and turbulent dissipation energy, respectively, and using Eq. (22). Both these calculated values correlate well with data obtained in a region 0.005–0.01 m above or below the impeller inside the flotation cell (Fig. 3). These relatively low values suggest that the mean vessel turbulent dissipation energy, rather than the local dissipation energy, determines the *mean* stability of the bubble–particle aggregates (Schulze, 1977). We note that a better fit of the experimental flotation rate constant was obtained with Eq. (22) (eddies of similar size as the bubbles) than with Eq. (21) (large eddies), especially in the decrease in flotation rate constant at large particle sizes and the production of a maximum at intermediate particle sizes. This indicates that turbulent eddies of size similar to that of the bubbles are more important than large eddies in the bubble–particle stability process.

Overall, the values of the calculated flotation rate constants in Fig. 2 are in a satisfactory agreement with the experimental data. More importantly, the characteristic shape of the flotation rate constant versus particle size curve is reproduced in these calculations.

Fig. 5 shows the contributions of collision, attachment and stability efficiencies (E_c, E_a, and E_s, respectively) to the flotation rate constants. The trends in E_c and E_s with particle diameter clearly explain the decrease in flotation rate constant for fine and coarse particles. As for E_a, the decrease of its value with increasing particle diameter follows the behaviour of quartz (Dai et al., 1999). Indeed, according to results in Fig. 4, the chalcopyrite particles in the MIM ore have a reasonably large

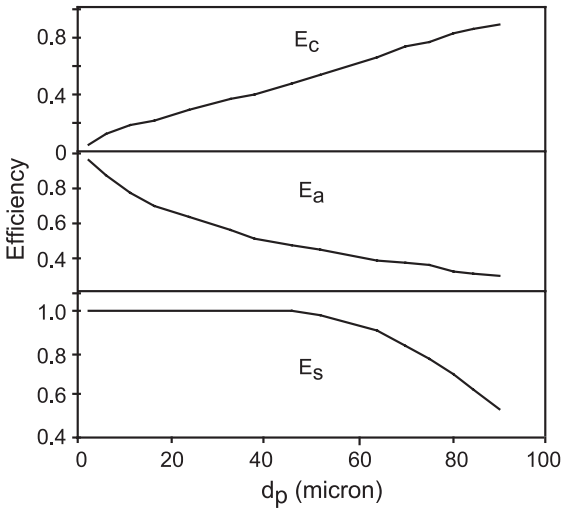

Fig. 5. Collision efficiency (E_c), attachment efficiency (E_a) and stability efficiency (E_s) as a function of particle diameter. Parameters used in the calculations are the same as those in Fig. 2.

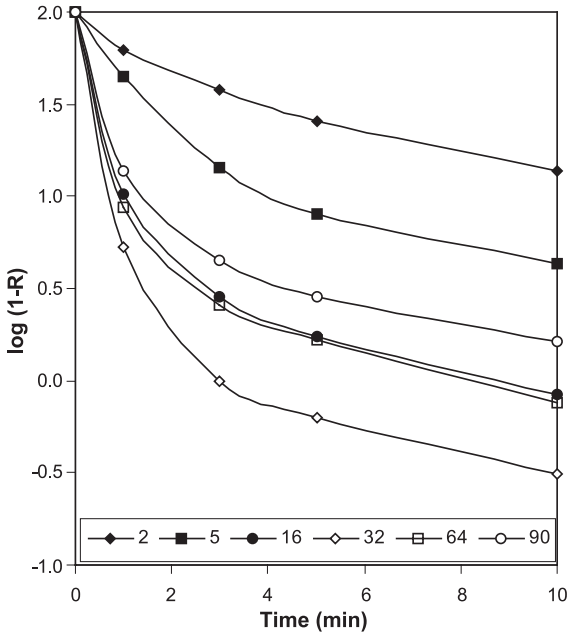

Fig. A1. Experimental data of log $(1-R)$ versus flotation time for chalcopyrite ore flotation for different average particle sizes in the flotation cell (particle size is in micrometer).

contact angle value of around $71 \pm 2°$, and therefore, they behave in a similar fashion to quartz particles of the same contact angle (Dai et al., 1999). Despite this apparent agreement, we caution that the hydrodynamic conditions inside the flotation cell in the present and earlier study (Dai et al., 1999) are certainly different. Therefore, more work is needed to identify the effects of fluid velocity and turbulence on induction time.

5. Conclusions

A flotation model was used to calculate the flotation rate constants of chalcopyrite particles in a complex sulfide ore as a function of particle diameter. This flotation model includes the contributions from the efficiencies of collision, attachment and stability between particles and bubbles as well as their frequency of collision. These calculated flotation rate constants were in satisfactory agreement with the flotation rate constants for chalcopyrite particles in an ore determined under turbulent flow conditions in a Rushton flotation cell. In particular, the relatively low flotation rate constants of fine and coarse chalcopyrite particles were reproduced and have been attributed to the low efficiency of collision and stability of these particles with bubbles, respectively. For these calculations, only the values of mean turbulent dissipation energy, bubble velocity and particle contact angle are required. The water advancing contact angle of the chalcopyrite particles in the ore was independently determined using a technique based upon Time of Flight Secondary Ion Mass spectroscopy. As for the turbulent dissipation energy, its optimum value used in the calculations corresponds to those measured in a region of relatively low turbulence inside the flotation cell close to the impeller. The optimum bubble velocity was found to be rather close to the bubble rising velocity, giving a good indication of the *relative* bubble velocity with respect to the "fluid" in the flotation cell.

Acknowledgements

The financial support for this work from the University of South Australia, the Australian Mineral Industries Research Association and the Australian Research Council, through the Special Research Centres Scheme, is gratefully acknowledged. Discussions with Prof. Roger Smart, Dr. Bill

Table A1
The fast (F_f) and slow (F_s) fractions and their corresponding rate constants obtained for the chalcopyrite ore flotation (e.g., after Crawford and Ralston, 1988), assuming that flotation is described. A double exponential: $1-R=F_f \exp(-k_f t)+F_s \exp(-k_s t)$. The flotation rate constant k is obtained from nonlinear regression based on the first-order equation $1-R=R_{max} \exp(-kt)$ (Eq. (23)), and is shown for comparison purposes

d (μm)	F_s	F_f	k_s	k_f	k (from Eq. (23))	R_{max}
2	0.47	0.53	0.125	0.5	0.5	0.84
6	0.14	0.86	0.12	0.78	0.86	0.94
11	0.06	0.94	0.14	1.33	1.36	0.97
16	0.033	0.97	0.13	2.76	2.44	0.98
33	0.012	0.99	0.14	3.33	3.07	0.99
46	0.019	0.98	0.17	3.45	3.02	0.99
64	0.037	0.96	0.16	2.86	2.64	0.98
91	0.046	0.95	0.1	2.29	2.18	0.97

Skinner and Dr. Stephen Grano are also sincerely appreciated.

Appendix A. Rate Constant Comparison

In Fig. A1, experimental data are shown for various size fractions of the chalcopyrite ore particles (the average particle diameter in micrometer is shown), i.e., ln $(1-R)$ versus time. This permits "fast" and "slow" component rate constants to be extracted. As is seen in Table A1, the fast rate constant correlates well with the value extracted from Eq. (23).

References

Abrahamson, J., 1975. Collision rates of small particles in a vigorously turbulent fluid. Chem. Eng. Sci. 30, 1371–1379.

Crawford, R., Ralston, J., 1988. The influence of particle and contact angle in mineral flotation. Int. J. Miner. Process. 23, 1–24.

Dai, Z., Dukhin, S., Fornasiero, D., Ralston, J., 1998. The inertial hydrodynamic interaction of particles and rising bubbles with mobile surfaces. J. Colloid Interface Sci. 197, 275–292.

Dai, Z., Fornasiero, D., Ralston, J., 1999. Particle–bubble attachment in mineral flotation. J. Colloid Interface Sci. 217, 70–76.

Dai, Z., Fornasiero, D., Ralston, J., 2000. Particle–bubble collision models—a review. Adv. Colloid Interface Sci. 85, 231–256.

Derjaguin, B.V., Dukhin, S.S., 1961. Theory of flotation of small and medium size particles. Trans. Inst. Min. Metall. 70, 221–246.

Dobby, G.S., Finch, J.A., 1987. Particle size dependence in flotation derived from a fundamental model of the capture process. Int. J. Miner. Process. 21, 241–260.

Dukhin, S.S., Kretschmar, G., Miller, R., 1995. Dynamics of adsorption at liquid interfaces: theory, experiment, application. In: Mobius, D., Miller, R. (Eds.), Studies in Interface Science. Elsevier, Amsterdam, The Netherlands, pp. 342–421.

Duineveld, P.C., 1995. The rise velocity and shape of bubbles in pure water at high Reynolds number. J. Fluid Mech. 292, 325–332.

Gorain, B.K., Franzidis, J.-P., Manlapig, E.V., 1996. Studies on impeller type, impeller speed and air flow rate in an industrial scale flotation cell: Part 3. Effect on superficial gas velocity. Miner. Eng. 9, 639–654.

Gorain, B.K., Franzidis, J.-P., Manlapig, E.V., 1997. Studies on impeller type, impeller speed and air flow rate in an industrial scale flotation cell: Part 4. Effect of bubble surface area flux on flotation performance. Miner. Eng. 10, 367–379.

Huh, C., Scriven, L.E.J., 1971. Hydrodynamic model of steady movement of a solid/liquid/fluid contact line. J. Colloid Interface Sci. 35 (1), 85–101.

Hui, S., 2001. Hydrodynamics of coarse-particle flotation. PhD Thesis, University of Newcastle.

Jameson, G.J., Nam, S., Young, M.M., 1977. Physical factors affecting recovery rates in flotation. Miner. Sci. Eng. 9 (3), 103–118.

Jenne, M., Reuss, M., 1999. A critical assessment on the use of 12-ε turbulence models for the simulation of turbulent liquid flow induced by a Rushton-turbine in baffled stirred tank reactors. Chem. Eng. Sci. 54, 3921–3941.

Jordan, C.E., Scheiner, B.J., 1990. Velocity profile measurements within a laboratory flotation cell. Fluid/Part. Sep. J. 3, 71–75.

Jordan, C.E., Spears, D.R., 1990. Evaluation of a turbulent flow model for fine bubble and fine particle flotation. Miner. Metall. Process., 65–73.

Jowett, A., 1980. Chapter 37 in fine particle processing. In: Somasundaran, P. (Ed.), Proc. Int. Symp. Fine particle processing, AIME, AIMM, New York.

Li, D., Fitzpatrick, J.A., Slattery, J.C., 1990. Rate of collection of particles by flotation. Ind. Eng. Chem. Res. 29 (6), 955–967.

Lynch, A.J., Johnson, N.J., Manlapig, E.V., Thorne, C.G., 1981. Mineral and Coal Flotation Circuits. Elsevier, Amsterdam.

Mular, A.L., Musara, W.T., 1991. Batch column flotation: rate data measurements. Proceedings of an International Conference on Column Flotation, Sudbury, Ontario, Canada, vol. 1, pp. 63–74.

Piantadosi, C., Smart, R.St.C., 2002. Statistical comparison of hydrophobic and hydrophilic species on galena and pyrite particles in flotation concentrates and tails from ToF-SIMS evidence. Int. J. Miner. Process. 64, 43–54.

Piantadosi, C., Jasieniak, M., Skinner, W.M., Smart, R.C., 2000. Statistical comparison of surface species in flotation concentrates and tails from ToF-SIMS evidence. Miner. Eng. 13 (13), 1377–1394.

Pyke, B.L., Fornasiero, D., Grano, S.R., Ralston, J., 2001. Prediction of the flotation rate of chalcopyrite particles in a copper ore. In: Finch, J.A., Rao, S.R., Huang, L. (Eds.), Interactions in Mineral Processing, COM 2001. Canadian Institute of Mining, Metallurgy and Petroleum, Montreal, Quebec.

Pyke, B.L., Fornasiero, D., Ralston, J., 2003. Bubble particle heterocoagulation under turbulent conditions. J. Colloid Interface Sci. (in press).

Ralston, J., 1992. In: Laskowski, J.S., Ralston, J. (Eds.), Chapter 6 in Colloid Chemistry in Minerals Processing. Elsevier, Amsterdam, pp. 203–223.

Rutherford, K., Lee, K.C., Mahmoudi, S.M.S., Yianneskis, M., 1996. Hydrodynamic characteristics of dual Rushton impeller stirred vessels. AIChE J. 42 (2), 332–346.

Sam, A., Gomez, C.O., Finch, J.A., 1996. Axial velocity profiles of single bubbles in water/frother solutions. Int. J. Miner. Process. 47, 177–196.

Schubert, H., 1999. On the turbulence-controlled microprocesses in flotation machines. Int. J. Miner. Process. 56, 257–276.

Schubert, H., Bischofberger, C., 1978. On the hydrodynamics of flotation machines. Int. J. Miner. Process. 5, 131–142.

Schulze, H.J., 1977. New theoretical and experimental investigation on stability of bubble/particle aggregates in flotation: a theory on the upper particle size of floatability. Int. J. Miner. Process. 4, 241–259.

Schulze, H.J., 1993. Flotation as a heterocoagulation process: pos-

sibilities of calculating the probability of flotation. Surfactant Science Series (Coagulation and Flocculation), vol. 47. Marcel Dekker, New York, pp. 321–354. Chapter 7.

Sutherland, K.L., 1948. Kinetics of the flotation process. J. Phys. Colloid 52, 394–425.

Wu, H., Patterson, G.K., 1989. Laser-doppler measurements of turbulent-flow parameters in a stirred mixer. Chem. Eng. Sci. 44 (10), 2207–2221.

Ye, Y., Miller, J.D., 1988. Bubble/particle contact time in the analysis of coal flotation. Coal Prep. 5, 147–166.